Effect of in-plane biaxial strains on the band structure of wurtzite GaN

B. Jogai
University Research Center, Wright State University, Dayton, Ohio 45435
(Received 9 June 1997)

The effect of strain on wurtzite GaN is studied theoretically using an sp^3d^5-sp^3 empirical tight-binding model. The model incorporates all nearest-neighbor and some second-nearest-neighbor interactions within the two-center approximation. The second-nearest-neighbor interactions excluded are the cation-cation interactions involving the Ga $3d$ orbital. Strain is included by scaling the two-center integrals appropriately. Thus the strain is modeled without invoking deformation potential theory, obviating the need for any additional parameters. The present model can accommodate any arbitrary strain orientation. The band structure has been calculated for in-plane biaxial strain. It is found that the band gap remains direct for in-plane biaxial strains ranging between $\pm 5\%$. Furthermore, the valence-band edge is of a different symmetry for tensile and compressive strains. The total density of states calculated via a fundamental numerical scheme is given for unstrained and strained GaN. [S0163-1829(98)06504-7]

I. INTRODUCTION

The wurtzite polytype of GaN is a promising material for applications as light-emitting diodes in the blue and ultraviolet wavelengths and as high-temperature electronic devices.[1] A great deal of effort has been directed at growing GaN thin films of a sufficiently high quality for practical use in these applications. Despite great strides in the growth, a number of problems remain unsolved.[2] One such problem arises from the lattice mismatch between bulk GaN and various substrates such as sapphire and SiC. This mismatch introduces large biaxial strains in the GaN epilayer. Additional strains arise from point defects and post-growth cooling.[2] A further complication is that the strains appear to be different for nominally identical growth conditions. Another is that the hexagonal growth columns have different axial orientations in the c plane. Consequently, the principal axes of the biaxial strains will vary from column to column. To better understand the strain, calculations of the strain-induced energy shifts of the band structure can prove useful in calibrating the strain through comparisons with photoreflectance and photoluminescence data.

In this paper, we present band-structure and density-of-states (DOS) calculations for wurtzite GaN under varying degrees of biaxial strain. The unstrained band structure of wurtzite GaN has been calculated by a number of authors[3–9] using *ab initio* pseudopotential techniques, and, in at least one such work[10] hydrostatic strain has been included. The band structure under compressive biaxial strain has also been calculated[11] using the $\mathbf{k}\cdot\mathbf{p}$ perturbation method within the cubic approximation.[12] The $\mathbf{k}\cdot\mathbf{p}$ method,[11] however, only gives the energies close to the Γ point and cannot reliably predict whether or not the fundamental energy gap is direct or indirect under various strains. The detailed behavior of the states in the Brillouin zone requires full-zone techniques such as *ab initio* pseudopotential[3–10] or empirical tight-binding (ETBM) methods. There have been very few published ETBM results on wurtzite nitrides. One of the earliest, to our knowledge, is that of Kobayashi *et al.*[13] on unstrained nitrides using the nearest-neighbor sp^3s^* method. More recently, Yang, Nakajima, and Sakai[14] have calculated the band structure of unstrained GaN and InN using an sp^3d^5-sp^3 ETBM, and Yang and Xu[15] have employed an sp^3s^* method with some second-nearest-neighbor interactions and included biaxial strain.

In the present work, the sp^3d^5-sp^3 ETBM model is extended to include strain. Both biaxial and uniaxial strains, as well as the simpler case of hydrostatic strain, are readily accommodated within the present model. Unlike $\mathbf{k}\cdot\mathbf{p}$ methods, the present ETBM model does not invoke deformation potential theory to include the strain. Except for the unstrained matrix elements, the only new parameters needed are the elements of the elastic stiffness tensor. The model is described in detail in Sec. II. Apart from the energy bands, the DOS is also of general interest. The DOS has a direct bearing on the luminescence and dielectric properties of the material and is an important element in the Fermi-Dirac statistics of the electrons and holes. Additionally, it plays a role in the calculation of the electronic specific heat. The total DOS is calculated using a first-principles numerical technique described in Sec. III. The band structure and DOS for unstrained and strained GaN are given in Sec. IV. The results are summarized in Sec. V.

II. STRAINED BAND-STRUCTURE CALCULATION

The band structure of strained wurtzite GaN is obtained via an sp^3d^5-sp^3 ETBM and is based on the one described recently by Yang, Nakajima, and Sakai[14] and extend in the present work to include strain. It is a standard ETBM, but adapted to the wurtzite symmetry with some additional refinements. Specifically, besides the conventional sp^3 basis on each atomic site, a d orbital is added to the basis set on the cation sites. With four atoms per unit cell, this leads to a 26×26 Hamiltonian. The justification for including the d state has been discussed by Yang, Nakajima, and Sakai[14] and is essential because of a near resonance between the Ga $3d$ and N $2s$ states.[16] All nearest-neighbor s, p, and d, and all second-nearest-neighbor s and p interactions are included within the two-center approximation.[17] The two-center ap-

proximation reduces the number of unknown matrix elements to five on-site one-center, eight nearest-neighbor two-center, and eight next-nearest-neighbor two-center integrals.

It is assumed that the displacement of any atom from the unstrained to the strained state can be expressed as a linear function of the coordinates, i.e., the strain is assumed to be homogeneous.[18] Any vector $\mathbf{x}'$ in the strained crystal can then be expressed in terms of a corresponding vector $\mathbf{x}$ in the unstrained crystal via

$$\mathbf{x}' = \mathbf{x} + \overleftrightarrow{\mathbf{e}} \cdot \mathbf{x}, \tag{1}$$

in which $\overleftrightarrow{\mathbf{e}}$ is the strain dyadic. From Eq. (1) and knowledge of $\overleftrightarrow{\mathbf{e}}$, all of the Slater-Koster[17] two-center integrals between atomic pairs can be worked out for any arbitrary strain orientation. The coordinate system is chosen as in Ref. 14 such that, before strain, the four atomic sites in the unit cell are chosen to lie in the y-z plane and the x-y plane chosen to coincide with the c plane. This ensures that the strain dyadic is diagonal for in-plane biaxial and uniaxial strains, the simplest cases of strain, apart from hydrostatic strain.

For in-plane biaxial strain, the six sides of the hexagon in the c plane are equally constrained by external forces so that

$$e_{xx} = e_{yy}. \tag{2}$$

The displacement along the c axis is then governed by minimum-energy requirements giving

$$e_{zz} = -\frac{2C_{13}}{C_{33}} e_{xx}, \tag{3}$$

where the C's are elements of the elastic stiffness tensor. Uniaxial strains can be included in a similar manner. Many orientations of in-plane uniaxial strain are possible. One possible form is to constrain any two parallel sides of the hexagon and allow all other displacements to relax according to minimum-energy requirements. Thus, if e_{xx} is fixed by external forces, the remaining elements of the strain dyadic will be given by

$$e_{yy} = -\frac{C_{13}(C_{11} - C_{12})}{C_{11}C_{33} - C_{13}^2} e_{xx} \tag{4}$$

and

$$e_{zz} = -\frac{C_{12}C_{33} - C_{13}^2}{C_{11}C_{33} - C_{13}^2} e_{xx}. \tag{5}$$

Following the notation of Yang, Nakajima, and Sakai,[14] the primitive translation vectors in rectangular coordinates are obtained from $\overleftrightarrow{\mathbf{e}}$ as follows: $\mathbf{a}_1 = [1(1+e_{xx}),0,0]$, $\mathbf{a}_2 = [-a/2(1+e_{xx}),\ \sqrt{3}a/2(1+e_{yy}),0]$, and $\mathbf{a}_3 = [0,0,c(1+e_{zz})]$, where a and c are the lattice constants. The atomic sites in the primitive cell are located at $\mathbf{t}_1 = [0,\sqrt{3}a/3(1+e_{yy}),7c/8(1+e_{zz})]$, $\mathbf{t}_2 = [0,0,0]$, $\mathbf{t}_3 = [0,0,3c/8(1+e_{zz})]$, and $\mathbf{t}_4 = [0,\sqrt{3}a/3(1+e_{yy}),c/2(1+e_{zz})]$, where $\mathbf{t}_1$ and $\mathbf{t}_3$ are the anion sites and $\mathbf{t}_2$ and $\mathbf{t}_4$ are the cation sites.

The integrals are worked out as prescribed in Ref. 17 and scaled according to Harrison's $1/d^2$ scaling rule.[19–21] An alternative scaling method has been suggested by Priester, Allan, and Lanoo,[22] in which a different scaling factor is used for each orbital pair and adjusted to fit experimental data. In the present work, we have elected to use the simpler Harrison rule[19–21] and justify it on the basis of very good fits to optical data when invoking this rule for type-II InAs/$In_xGa_{1-x}Sb$ (Ref. 23) and ZnS/ZnSe strained-layer superlattices.[24] This approximation has also been successfully used to study heterointerface bond relaxation for a wide range of semiconductor interfaces.[25] The matrix elements $(ll'm)$ are given by

$$(ll'm) = \frac{\hbar^2}{m_0} \eta_{ll'm}, \tag{6}$$

where m_0 is the free-electron mass and $\eta_{ll'm}$ is the normalized Harrison matrix element.[21] The definition of $(ll'm)$ in Eq. (6) differs from Ref. 14, since the interatomic distances are already explicitly given in the matrix elements described in the foregoing. The matrix elements $\eta_{ll'm}$ are listed in Table IV of Ref. 14. The elastic constants are taken from Ref. 26.

III. DENSITY-OF-STATES CALCULATION

The total DOS $D(\hbar\omega)$ is given by

$$D(\hbar\omega) = \frac{2}{(2\pi)^3} \sum_3 \int \frac{dS}{|\nabla_{\mathbf{k}} E_n(\mathbf{k})|_{E_n(\mathbf{k})=\hbar\omega}}, \tag{7}$$

where dS represents an element of surface in $\mathbf{k}$ space on the surface defined by $E_n(\mathbf{k}) = \hbar\omega$ and $E_n(\mathbf{k})$ represents the nth energy band. Equation (7) is evaluated via the Lehmann-Taut[27] (LT) numerical algorithm. An alternative scheme is the Gilat-Raubenheimer[28] (GR) method. We have chosen the LT over the GR method for its higher accuracy,[27] though for total DOS calculations, we have found GR results to be $<0.1\%$ of LT results, a negligible difference. The LT scheme, however, has the advantage of being able to evaluate more complex integrands[29] and can accommodate grids with different k_x, k_y, and k_z spacings, whereas the GR method is constrained to cubic meshes. Within the LT scheme, the irreducible part of the first Brillouin zone is divided into a tetrahedral mesh comprising of approximately 125 000 $\mathbf{k}$ points, from which are derived approximately 350 000 tetrahedrons, and the band structure calculated at the corners of each tetrahedron. An energy histogram is formed with a grid separation of about 3.5 meV. For each energy surface, the area of intersection with each tetrahedron is evaluated and the results summed over all the tetrahedrons and all the bands. The final result is a histogram of D versus $\hbar\omega$.

IV. RESULTS AND DISCUSSION

Figure 1 shows the band structure of unstrained wurtzite GaN. As expected, it is identical to the results of Yang, Nakajima, and Sakai.[14] Though not visible on the scale of Fig. 1, the valence band at the Γ point is already split, even without strain, into a fourfold degenerate band transforming as Γ_5 about 7.8 meV above a twofold degenerate band trans-

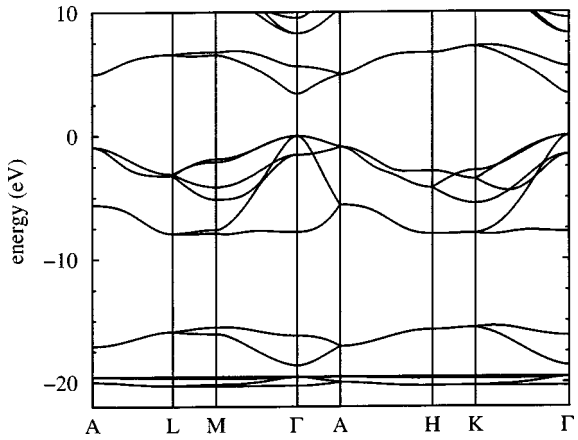

FIG. 1. Band structure of unstrained wurtzite GaN.

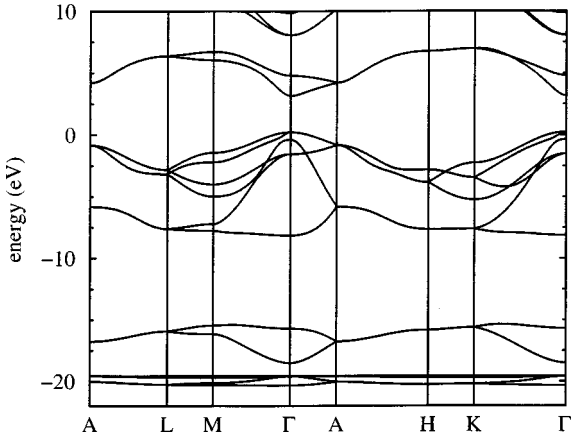

FIG. 3. Band structure of wurtzite GaN under 5% (tensile) biaxial strain in the c plane.

forming as γ_1. These designations are described in detail by Bir and Pikus.[12] To understand this result, it should be noted that tetrahedral bonding of the nearest-neighbor atomic pairs occurs when $c/a=(8/3)^{1/2}$. In the absence of crystal-field and spin-orbit splittings, the valence-band edge should be sixfold degenerate, transforming as Γ_4'.[30] Based on experimental data, $c/a=1.6259$, differing slightly but noticeably from ideality. Ignoring second-nearest-neighbor interactions for the moment, this deviation from tetrahedral symmetry effectively introduces a nearest-neighbor crystal field that splits the Γ_5 and Γ_1 states by about 17.5 meV. When included, the second-nearest-neighbor interactions effectively introduce an additional crystal field that, in this particular instance, acts in an opposite manner. Instead of the above experimental ratio, if $c/a>(8/3)^{1/2}$, the Γ_5 band would lie below the Γ_1 band within the present ETBM model.

Figure 2 shows the band structure of GaN under a 5% in-plane compressive strain, the plane in question being the c plane. As expected, the band gap at the Γ point increases. Additionally, the separation between the Γ_5 and Γ_1 valence bands increases, as the Γ_1 valence band now becomes the valence-band minimum. The Γ_1 valence and Γ_1 conduction bands remain direct. Figure 3 shows the band structure of GaN under a 5% in-plane tensile strain. The band gap is smaller relative to that of Fig. 1 and the valence-band minimum is now the fourfold degenerate Γ_5 state. It is also found that $|\Gamma_{1v}-\Gamma_{5v}|$ increases with the magnitude of the strain regardless of whether the strain is tensile or compressive. These results are consistent with the total-energy pseudopotential calculations of Majewski, Städele, and Vogl,[31] which also show a change in character of the valence-band edge at certain values of strain. As will be seen shortly, our results differ, however, from the sp^3s^* ETBM of Yang and Xu.[15] The model of Yang and Xu[15] incorporates all nearest-neighbor s,p and s^* interactions but includes only the s^*-p second-nearest-neighbor interactions.

Figure 4 shows the effective band gap over a range of compressive and tensile strains. The change in slope of the band gap near zero strain is caused by the anticrossing of the Γ_1 and Γ_5 valence bands. The conduction- and valence-band minima remain at the Γ point over a wider range of strains than shown in Fig. 4, in contrast to the results of Ref. 15. Additionally, the band gap in the present work depends on

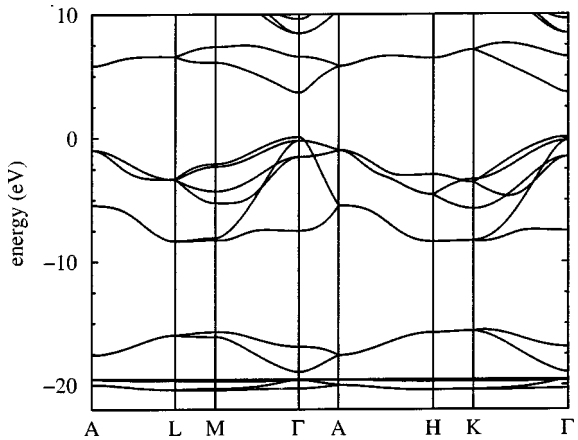

FIG. 2. Band structure of wurtzite GaN under −5% (compressive) biaxial strain in the c plane.

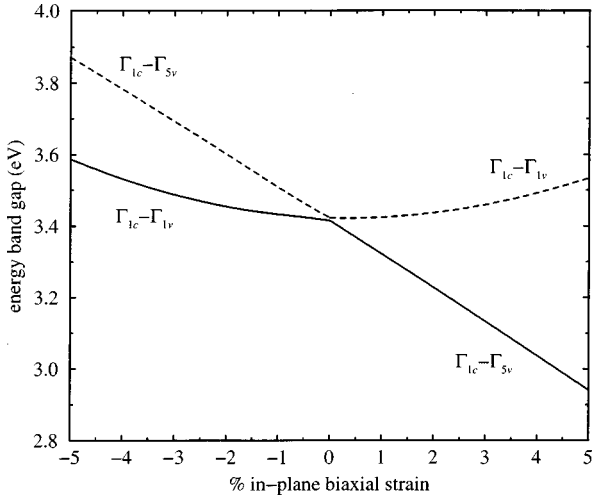

FIG. 4. Band gap of wurtzite GaN as a function of % biaxial strain in the c plane. The negative sign denotes compressive and the positive sign tensile strain. The x axis denotes $e_{xx}=e_{yy}$ described in Sec. II. The states from which the band gap is calculated are indicated. The solid curve is the gap between the Γ_{1c} conduction band and the highest valence band and the dashed curve the gap between the Γ_{1c} conduction band and the next-highest valence band.

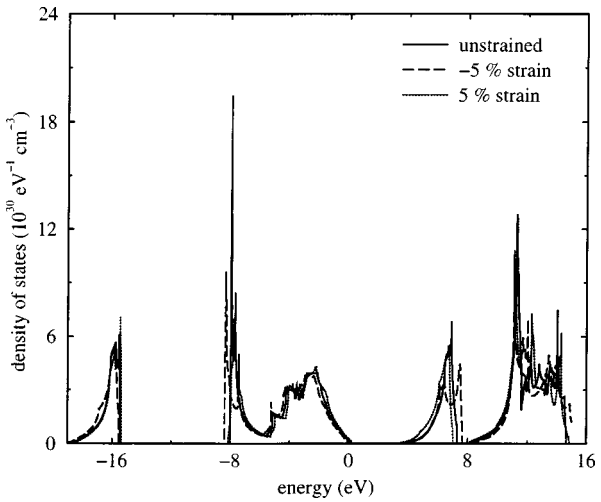

FIG. 5. Total DOS for unstrained and strained wurtzite GaN excluding the *d* states. The dashed line indicates compressive biaxial strain and the dotted line tensile biaxial strain. States above 15 eV are not shown.

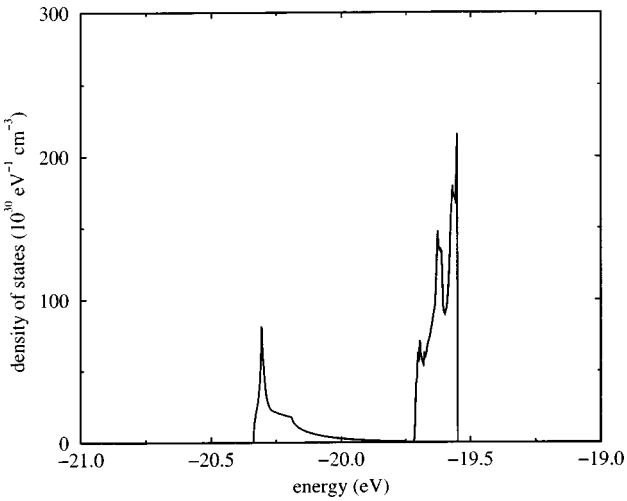

FIG. 6. Total DOS for unstrained wurtzite GaN showing only the *d* states.

both the magnitude and *sign* of the strain, as one would expect from the change in volume of the unit cell. In Ref. 15, however, it is seen that the band gap increases under *both* tensile and compressive strains, in contrast to the present results. Such a result could, conceivably, be anomalous. One possible reason is that the bond relaxation of the *c*-axis nearest-neighbor bond is disallowed in Ref. 15: the *c*-axis bond is forced to assume the same length as the remaining three nearest-neighbor bonds for all strains, and only the bond angles are allowed to relax. The present work allows for a full relaxation of all bond lengths and bond angles through Eq. (1). We believe that if the *c*-axis bond relaxation were allowed within the sp^2s^* ETBM, the results would be very similar to the present sp^3d^5-sp^3 ETBM results. Qualitative support for the results of Fig. 4 can be found in the PR measurements of Shikanai *et al.*[32] and Chichibu *et al.*[33] of the exciton spectra of wurtzite GaN epilayers under varying biaxial strain. The PR data[32,33] also show clear evidence of a turning point at a certain strain, an indication, we believe, of a change in character of the valence-band edge. A quantitative comparison with the PR data[32,33] would require the inclusion of the spin-orbit interaction and its coupling with both the crystal field and the strain. These effects have not yet been included in the present work.

Figure 5 shows the total DOS for unstrained and strained GaN. Because of strong localization of the Ga 3*d* band (see Figs. 1–3), its DOS is an order of magnitude greater than that of the other valence bands and is shown separately in Fig. 6. It has relatively fewer features than the other states shown in Fig. 5. From Eq. (7), it is seen that the only critical points to be expected are of the type $\nabla_{\mathbf{k}} E_n(\mathbf{k}) = 0$, generally occurring at high symmetry points in the Brillouin zone. Besides maxima and minima, Van Hove singularities of type S_1 and S_2 are both present, as required by Van Hove's theorem.[34] If the tetrahedrons and energy grid are too large (see Sec. III), the S_1 and S_2 saddle points are either reproduced incorrectly or not at all. It is noted that the changes in the DOS with strain are quite pronounced, particularly in the conduction bands and the lowest valence bands. Only small changes are seen in the highest valence band.

V. SUMMARY AND CONCLUSIONS

An ETBM has been used to study the band structure of wurtzite GaN under biaxial strains. The model employs an sp^3d^5 basis on the cation site and an sp^3 basis on the anion site with up to second-nearest-neighbor interactions. It is found that the fundamental energy gap remains direct over a range of strain of $\pm 5\%$, though a change in symmetry occurs at the valence-band minimum for tensile strain. Under compressive strain, the band gap increases relative to the unstrained result. The results are reversed for tensile strain. Contrary to previous results, it is seen that the band gap *does* depend on the sign of the strain. A detailed calculation of the total DOS has been presented for unstrained and strained GaN. These results are based on directly solving the DOS integral via the LT method.

ACKNOWLEDGMENTS

The author is indebted to C. W. Litton and C. I. Huang for technical support and D. N. Talwar, D. C. Reynolds, and C. E. Stutz for helpful discussions. This work was partially supported by AFOSR and performed at Wright Laboratory, Avionics Directorate (WL/AADP), Wright Patterson Air Force Base under USAF Contract No. F33615-95-C-1619.

[1] S. Strite and H. Morkoç, J. Vac. Sci. Technol. B **10**, 1237 (1992).
[2] C. Kisielowski, J. Krüger, S. Ruvimov, T. Suski, J. W. Ager III, E. Jones, Z. Lilental-Weber, M. Rubin, E. R. Weber, M. D. Bremser, and R. F. Davis, Phys. Rev. B **54**, 17 745 (1996).
[3] M. Z. Zhu and W. Y. Ching, J. Phys. Chem. Solids **46**, 977 (1984).
[4] M. Palummo, C. M. Bertoni, L. Reining, and F. Finocchi, Physica B **185**, 404 (1993).
[5] K. Miwa and A. Fukumoto, Phys. Rev. B **48**, 7897 (1993).
[6] S. J. Jenkins, G. P. Srivastava, and J. C. Inkson, J. Phys.: Condens. Matter **6**, 8781 (1994).
[7] M. Suzuki, T. Uenoyama, and A. Yanase, Phys. Rev. B **52**, 8132 (1995).
[8] S. H. Jhi and J. Ihm, Phys. Status Solidi B **191**, 387 (1995).
[9] M. Suzuki and T. Uenoyama, Jpn. J. Appl. Phys., Part 1 **34**, 3442 (1995).
[10] N. E. Christensen and I. Gorczyca, Phys. Rev. B **50**, 4397 (1994).
[11] S. L. Chuang and C. S. Chang, Phys. Rev. B **54**, 2491 (1996).
[12] G. L. Bir and G. E. Pikus, *Symmetry and Strain-Induced Effects in Semiconductors* (Halsted, New York, 1974).
[13] A. Kobayashi, O. F. Sankey, S. M. Volz, and J. D. Dow, Phys. Rev. B **28**, 935 (1983).
[14] T. Yang, S. Nakajima, and S. Sakai, Jpn. J. Appl. Phys., Part 1 **34**, 5913 (1995).
[15] Z. Yang and Z. Xu, Phys. Rev. B **54**, 17 577 (1996).
[16] V. Fiorentini, M. Methfessel, and M. Scheffler, Phys. Rev. B **47**, 13 353 (1993).
[17] J. C. Slater and G. F. Koster, Phys. Rev. **94**, 1498 (1954).
[18] A. E. H. Love, *A Treatise on the Mathematical Theory of Elasticity*, 4th ed. (Dover, New York, 1944), Chap. 1.
[19] W. A. Harrison, Phys. Rev. B **14**, 702 (1976).
[20] W. A. Harrison and S. T. Pantilides, Phys. Rev. B **14**, 691 (1976).
[21] W. A. Harrison, *Electronic Structure and the Properties of Solids* (Dover, New York, 1989).
[22] C. Priester, G. Allan, and M. Lanoo, Phys. Rev. B **37**, 8519 (1988).
[23] D. N. Talwar, J. P. Loehr, and B. Jogai, Phys. Rev. B **49**, 10 345 (1994).
[24] Y. Wu, S. Fujita, and S. Fujita, J. Appl. Phys. **67**, 908 (1990).
[25] E. Yamaguchi, J. Phys. Soc. Jpn. **57**, 2461 (1988).
[26] *Semiconductors—Basic Data*, 2nd revised ed., edited by O. Madelung (Springer, Berlin, 1996).
[27] G. Lehmann and M. Taut, Phys. Status Solidi B **54**, 469 (1972).
[28] G. Gilat and L. J. Raubenheimer, Phys. Rev. **144**, 390 (1966); **147**, 670(E) (1966).
[29] B. Jogai and D. N. Talwar, Phys. Rev. B **54**, 14 524 (1996).
[30] D. C. Reynolds and T. C. Collins, *Excitons—Their Properties and Uses* (Academic, New York, 1981).
[31] J. A. Majewski, M. Städele, and P. Vogl, MRS Internet J. Nitride Semicond. Res. **1**, 30 (1996).
[32] A. Shikanai, T. Azuhata, T. Sota, S. Chichibu, A. Kuramata, K. Horino, and S Nakamura, J. Appl. Phys. **81**, 417 (1997).
[33] S. Chichibu, T. Azuhata, T. Sota, H. Amano, and I. Akasaki, Appl. Phys. Lett. **70**, 2085 (1997).
[34] J. M. Ziman, *Principles of the Theory of Solids* (Cambridge University Press, Cambridge, 1979).